



Measurement of the polarization amplitudes and triple product asymmetries in the $B_s^0 \rightarrow \phi\phi$ decay [☆]

LHCb Collaboration

ARTICLE INFO

Article history:

Received 16 April 2012

Received in revised form 12 May 2012

Accepted 6 June 2012

Available online 9 June 2012

Editor: W.-D. Schlatter

ABSTRACT

Using 1.0 fb⁻¹ of pp collision data collected at a centre-of-mass energy of $\sqrt{s} = 7$ TeV with the LHCb detector, measurements of the polarization amplitudes, strong phase difference and triple product asymmetries in the $B_s^0 \rightarrow \phi\phi$ decay mode are presented. The measured values are

$$|A_0|^2 = 0.365 \pm 0.022 \text{ (stat)} \pm 0.012 \text{ (syst)},$$

$$|A_{\perp}|^2 = 0.291 \pm 0.024 \text{ (stat)} \pm 0.010 \text{ (syst)},$$

$$\cos(\delta_{\parallel}) = -0.844 \pm 0.068 \text{ (stat)} \pm 0.029 \text{ (syst)},$$

$$A_U = -0.055 \pm 0.036 \text{ (stat)} \pm 0.018 \text{ (syst)},$$

$$A_V = 0.010 \pm 0.036 \text{ (stat)} \pm 0.018 \text{ (syst)}.$$

© 2012 CERN. Published by Elsevier B.V. Open access under [CC BY-NC-ND license](#).

1. Introduction

In the Standard Model, the flavour-changing neutral current decay $B_s^0 \rightarrow \phi\phi$ proceeds via a $b \rightarrow s\bar{s}s$ penguin process. Studies of the polarization amplitudes and triple product asymmetries in this decay provide powerful tests for the presence of contributions from processes beyond the Standard Model [1–5].

The $B_s^0 \rightarrow \phi\phi$ decay is a pseudoscalar to vector–vector transition. As a result, there are three possible spin configurations of the vector meson pair allowed by angular momentum conservation. These manifest themselves as three helicity states, with amplitudes denoted H_{+1} , H_{-1} and H_0 . It is convenient to define linear polarization amplitudes, which are related to the helicity amplitudes through the following transformations

$$\begin{aligned} A_0 &= H_0, \\ A_{\perp} &= \frac{H_{+1} - H_{-1}}{\sqrt{2}}, \\ A_{\parallel} &= \frac{H_{+1} + H_{-1}}{\sqrt{2}}. \end{aligned} \quad (1)$$

The $\phi\phi$ final state can be a mixture of CP -even and CP -odd eigenstates. The longitudinal (A_0) and parallel (A_{\parallel}) components are CP -even and the perpendicular component (A_{\perp}) is CP -odd. From the V - A structure of the weak interaction, the longitudinal component, $f_L = |A_0|^2 / (|A_0|^2 + |A_{\perp}|^2 + |A_{\parallel}|^2)$, is expected to be

dominant [6–8]. However, roughly equal longitudinal and transverse components are found in measurements of $B^+ \rightarrow \phi K^{*+}$, $B^0 \rightarrow \phi K^{*0}$, $B^+ \rightarrow \rho^0 K^{*+}$ and $B^0 \rightarrow \rho^0 K^{*0}$ decays at the B-factories [9–14]. To explain this, large contributions from either penguin annihilation effects [15] or final state interactions [16] have been proposed. Recent calculations where phenomenological parameters are adjusted to account for the data allow f_L in the range 0.4–0.7 [6,7]. Another pseudoscalar to vector–vector penguin decay is $B_s^0 \rightarrow K^{*0} \bar{K}^{*0}$. A recent measurement by the LHCb Collaboration in this decay mode has found a value of $f_L = 0.31 \pm 0.12 \pm 0.04$ [17].

The time-dependent differential decay rate for the $B_s^0 \rightarrow \phi\phi$ mode can be written as

$$\frac{d^4 \Gamma}{d \cos \theta_1 d \cos \theta_2 d \Phi dt} \propto \sum_{i=1}^6 K_i(t) f_i(\theta_1, \theta_2, \Phi), \quad (2)$$

where the helicity angles $\Omega = (\theta_1, \theta_2, \Phi)$ are defined in Fig. 1. The angular functions $f_i(\Omega)$ are [18]

$$\begin{aligned} f_1(\theta_1, \theta_2, \Phi) &= 4 \cos^2 \theta_1 \cos^2 \theta_2, \\ f_2(\theta_1, \theta_2, \Phi) &= \sin^2 \theta_1 \sin^2 \theta_2 (1 + \cos 2\Phi), \\ f_3(\theta_1, \theta_2, \Phi) &= \sin^2 \theta_1 \sin^2 \theta_2 (1 - \cos 2\Phi), \\ f_4(\theta_1, \theta_2, \Phi) &= -2 \sin^2 \theta_1 \sin^2 \theta_2 \sin 2\Phi, \\ f_5(\theta_1, \theta_2, \Phi) &= \sqrt{2} \sin 2\theta_1 \sin 2\theta_2 \cos \Phi, \\ f_6(\theta_1, \theta_2, \Phi) &= -\sqrt{2} \sin 2\theta_1 \sin 2\theta_2 \sin \Phi. \end{aligned} \quad (3)$$

The time-dependent functions $K_i(t)$ are given in [19]

[☆] © CERN for the benefit of the LHCb Collaboration.

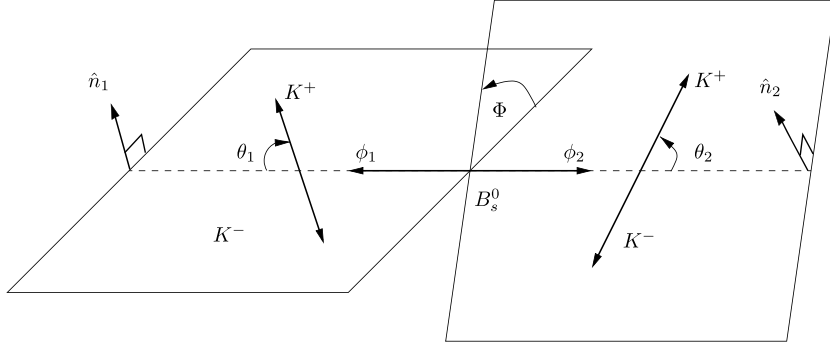


Fig. 1. Decay angles for the $B_s^0 \rightarrow \phi\phi$ decay, where the K^+ momentum in the $\phi_{1,2}$ rest frame, and the parent $\phi_{1,2}$ momentum in the rest frame of the B_s^0 meson span the two ϕ meson decay planes, $\theta_{1,2}$ is the angle between the K^+ track momentum in the $\phi_{1,2}$ meson rest frame and the parent $\phi_{1,2}$ momentum in the B_s^0 rest frame, Φ is the angle between the two ϕ meson decay planes and $\hat{n}_{1,2}$ is the unit vector normal to the decay plane of the $\phi_{1,2}$ meson.

$$\begin{aligned}
K_1(t) &= \frac{1}{2} A_0^2 [(1 + \cos \phi_s) e^{-\Gamma_L t} + (1 - \cos \phi_s) e^{-\Gamma_H t} \\
&\quad \pm 2e^{-\Gamma_s t} \sin(\Delta m_s t) \sin \phi_s], \\
K_2(t) &= \frac{1}{2} A_{\parallel}^2 [(1 + \cos \phi_s) e^{-\Gamma_L t} + (1 - \cos \phi_s) e^{-\Gamma_H t} \\
&\quad \pm 2e^{-\Gamma_s t} \sin(\Delta m_s t) \sin \phi_s], \\
K_3(t) &= \frac{1}{2} A_{\perp}^2 [(1 - \cos \phi_s) e^{-\Gamma_L t} + (1 + \cos \phi_s) e^{-\Gamma_H t} \\
&\quad \mp 2e^{-\Gamma_s t} \sin(\Delta m_s t) \sin \phi_s], \\
K_4(t) &= |A_{\parallel}| |A_{\perp}| \left[\pm e^{-\Gamma_s t} \{ \sin \delta_1 \cos(\Delta m_s t) \right. \\
&\quad \left. - \cos \delta_1 \sin(\Delta m_s t) \cos \phi_s \} \right. \\
&\quad \left. - \frac{1}{2} (e^{-\Gamma_H t} - e^{-\Gamma_L t}) \cos \delta_1 \sin \phi_s \right], \\
K_5(t) &= \frac{1}{2} |A_0| |A_{\parallel}| \cos(\delta_2 - \delta_1) \\
&\quad \times [(1 + \cos \phi_s) e^{-\Gamma_L t} + (1 - \cos \phi_s) e^{-\Gamma_H t} \\
&\quad \pm 2e^{-\Gamma_s t} \sin(\Delta m_s t) \sin \phi_s], \\
K_6(t) &= |A_0| |A_{\perp}| \left[\pm e^{-\Gamma_s t} \{ \sin \delta_2 \cos(\Delta m_s t) \right. \\
&\quad \left. - \cos \delta_2 \sin(\Delta m_s t) \cos \phi_s \} \right. \\
&\quad \left. - \frac{1}{2} (e^{-\Gamma_H t} - e^{-\Gamma_L t}) \cos \delta_2 \sin \phi_s \right], \quad (4)
\end{aligned}$$

where the upper of the \pm or \mp signs refers to the B_s^0 meson and the lower refers to a \bar{B}_s^0 meson. Here, Γ_L and Γ_H are the decay widths of the light and heavy B_s^0 mass eigenstates,¹ Δm_s is the B_s^0 oscillation frequency, $\delta_1 = \arg(A_{\perp}/A_{\parallel})$ and $\delta_2 = \arg(A_{\perp}/A_0)$ are CP -conserving strong phases and ϕ_s is the weak CP -violating phase. It is assumed that the weak phases of the three polarization amplitudes are equal. The quantities Γ_H and Γ_L correspond to the observables $\Delta\Gamma_s = \Gamma_L - \Gamma_H$ and $\Gamma_s = (\Gamma_L + \Gamma_H)/2$. In the Standard Model, the value of ϕ_s for this mode is expected to be very close to zero due to a cancellation between the phases arising from mixing and decay [20].² A calculation based on QCD factorization provides an upper limit of 0.02 rad for ϕ_s [21,6]. This is different to the

situation in the $B_s^0 \rightarrow J/\psi\phi$ decay, where the Standard Model predicts $\phi_s(J/\psi\phi) = -2 \arg(-V_{ts}V_{tb}^*/V_{cs}V_{cb}^*) = -0.036 \pm 0.002$ rad [22]. The magnitude of both weak phase differences can be enhanced in the presence of new physics in B_s^0 mixing, where recent results from LHCb have placed stringent constraints [23]. For the $B_s^0 \rightarrow \phi\phi$ decay, new particles could also contribute in $b \rightarrow s$ penguin loops.

To measure the polarization amplitudes, a time-integrated untagged analysis is performed, assuming that an equal number of B_s^0 and \bar{B}_s^0 mesons are produced and that the CP -violating phase is zero as predicted in the Standard Model.³ In this case, the functions $K_i(t)$ integrate to

$$\begin{aligned}
K_1 &= |A_0|^2 / \Gamma_L, \\
K_2 &= |A_{\parallel}|^2 / \Gamma_L, \\
K_3 &= |A_{\perp}|^2 / \Gamma_H, \\
K_4 &= 0, \\
K_5 &= |A_0| |A_{\parallel}| \cos(\delta_{\parallel}) / \Gamma_L, \\
K_6 &= 0, \quad (5)
\end{aligned}$$

where the strong phase difference is defined by $\delta_{\parallel} \equiv \delta_2 - \delta_1 = \arg(A_{\parallel}/A_0)$ and the time integration assumes uniform time acceptance.

In addition, a search for physics beyond the Standard Model is performed by studying the triple product asymmetries [1–3] in the $B_s^0 \rightarrow \phi\phi$ decay. Non-zero values of these quantities can be either due to T -violation or final-state interactions. Assuming CPT conservation, the former case implies that CP is violated. Experimentally, the extraction of the triple product asymmetries is straightforward and provides a measure of CP violation that does not require flavour tagging or a time-dependent analysis.

There are two observable triple products denoted $U = \sin(2\Phi)/2$ and $V = \pm \sin(\Phi)$, where the positive sign is taken if the T -even quantity $\cos \theta_1 \cos \theta_2 \geq 0$ and the negative sign otherwise. These variables correspond to the T -odd triple products

$$\begin{aligned}
\sin \Phi &= (\hat{n}_1 \times \hat{n}_2) \cdot \hat{p}_1, \\
\sin(2\Phi)/2 &= (\hat{n}_1 \cdot \hat{n}_2)(\hat{n}_1 \times \hat{n}_2) \cdot \hat{p}_1, \quad (6)
\end{aligned}$$

where \hat{n}_i ($i = 1, 2$) is a unit vector perpendicular to the ϕ_i decay plane and \hat{p}_1 is a unit vector in the direction of the ϕ_1 momentum

¹ Units are adopted such that $\hbar = 1$.

² The convention used in this Letter is that the symbol ϕ_s refers solely to the weak phase difference measured in the $B_s^0 \rightarrow \phi\phi$ decay.

³ In the case of non-zero ϕ_s deviations from these formulas are suppressed by a factor of $\Delta\Gamma_s/\Gamma_s$ and hence only small variations would be observed on the fitted parameters.

in the B_s^0 rest frame. The triple products, U and V , are proportional to the f_4 and f_6 angular functions which, for $\phi_s = 0$, vanish in the untagged decay rate for any value of t . The f_4 and f_6 angular functions would not vanish in the presence of new physics processes that cause the polarization amplitudes to have different weak phases [1]. Therefore, a measurement of significant asymmetries would be an unambiguous signal for the effects of new physics [1,3].

The asymmetry, A_U , is defined as

$$A_U = \frac{N_+ - N_-}{N_+ + N_-}, \quad (7)$$

where N_+ (N_-) is the number of events with $U > 0$ ($U < 0$). Similarly A_V is defined as

$$A_V = \frac{M_+ - M_-}{M_+ + M_-}, \quad (8)$$

where M_+ (M_-) is the number of events with $V > 0$ ($V < 0$). The triple product asymmetries, A_U and A_V are proportional to the interference terms $\mathcal{I}m(A_{\perp} A_{\parallel}^*)$ and $\mathcal{I}m(A_{\perp} A_0^*)$ in the decay rate.

The $B_s^0 \rightarrow \phi\phi$ decay mode was first observed by the CDF Collaboration [24]. More recently, CDF has reported measurements of the polarization amplitudes and triple product asymmetries in this mode based on a sample of 295 events [25]. In this Letter, measurements of the polarization amplitudes, $|A_0|^2$ and $|A_{\perp}|^2$, the strong phase difference, δ_{\parallel} , and the triple product asymmetries, A_U and A_V , are presented. The dataset consists of 801 ± 29 candidates collected in 1.0 fb^{-1} of pp collisions at the LHC. The Monte Carlo (MC) simulation samples used are based on the PYTHIA 6.4 generator [26] configured with the parameters detailed in Ref. [27]. The EVTGEN [28] and GEANT4 [29] packages are used to generate hadron decays and simulate interactions in the detector, respectively.

2. Detector description

The LHCb detector [30] is a single-arm forward spectrometer covering the pseudorapidity range $2 < \eta < 5$, designed for the study of particles containing b or c quarks. The detector includes a high precision tracking system consisting of a silicon-strip vertex detector surrounding the pp interaction region, a large-area silicon-strip detector located upstream of a dipole magnet with a bending power of about 4 Tm, and three stations of silicon-strip detectors and straw drift-tubes placed downstream. The combined tracking system has a momentum resolution $\Delta p/p$ that varies from 0.4% at 5 GeV/c to 0.6% at 100 GeV/c, and an impact parameter resolution of 20 μm for tracks with high transverse momentum. Charged hadrons are identified using two ring-imaging Cherenkov detectors. Photon, electron and hadron candidates are identified by a calorimeter system consisting of scintillating-pad and pre-shower detectors, an electromagnetic calorimeter and a hadronic calorimeter. Muons are identified by a muon system composed of alternating layers of iron and detector stations. The trigger consists of a hardware stage, based on information from the calorimeter and muon systems, followed by a software stage which applies a full event reconstruction.

The software trigger used in this analysis requires a two-, three- or four-track secondary vertex with a high sum of the transverse momentum, p_T , of the tracks, significant displacement from the primary interaction, and at least one track with $p_T > 1.7 \text{ GeV}/c$; impact parameter ξ^2 with respect to the primary interaction greater than 16; and a track fit $\xi^2/\text{ndf} < 2$ where ndf is the number of degrees of freedom in the track fit. A multivariate algorithm is used for the identification of the secondary

Table 1

Selection criteria for the $B_s^0 \rightarrow \phi\phi$ decay. The abbreviation IP stands for impact parameter and $p_T^{\phi 1}$ and $p_T^{\phi 2}$ refer to the transverse momentum of the two ϕ candidates.

Variable	Value
Track χ^2/ndf	< 5
Track p_T	$> 500 \text{ MeV}/c$
Track IP χ^2	> 21
$\Delta \ln \mathcal{L}_{K\pi}$	> 0
$ M_{\phi} - M_{\phi}^{\text{PDG}} $	$< 12 \text{ MeV}/c^2$
$p_T^{\phi 1} \cdot p_T^{\phi 2}$	$> 900 \text{ MeV}/c$
$p_T^{\phi 1} \cdot p_T^{\phi 2}$	$> 2 \text{ GeV}^2/c^2$
ϕ vertex χ^2/ndf	< 24
B_s^0 vertex χ^2/ndf	< 7.5
B_s^0 vertex separation χ^2	> 270
B_s^0 IP χ^2	< 15

vertices [31]. The $B_s^0 \rightarrow \phi\phi$ candidates are selected with high efficiency either by identifying events containing a ϕ meson or using topological information to select hadronic b decays. Events passing the software trigger are stored for subsequent offline processing.

3. Event selection

The $B_s^0 \rightarrow \phi\phi$ channel is reconstructed using events where both ϕ mesons decay into a K^+K^- pair. The $B_s^0 \rightarrow \phi\phi$ selection criteria were optimized using a data-driven approach based on the sP lot technique employing the four-kaon mass as the unfolding variable [32] to separate signal (S) and background (B) with the aim of maximizing $S/\sqrt{S+B}$. The resulting cuts are summarized in Table 1. Good quality track reconstruction is ensured by a cut on the transverse momentum (p_T) of the daughter particles and a cut on the χ^2/ndf of the track fit.

Combinatorial background is reduced by cuts on the minimum impact parameter significance of the tracks with respect to all reconstructed pp interaction vertices and also by imposing a requirement on the vertex separation χ^2 of the B_s^0 candidate. Well-identified ϕ meson candidates are selected by requiring that the two particles involved are identified as kaons by the ring-imaging Cherenkov detectors using a cut on the difference in the global likelihood between the kaon and pion hypotheses ($\Delta \ln \mathcal{L}_{K\pi} > 0$) and by requiring that the reconstructed mass of each K^+K^- pair is within $12 \text{ MeV}/c^2$ of the nominal mass of the ϕ meson [33]. Further signal purity is achieved by cuts on the transverse momentum of the ϕ candidates.

Fig. 2 shows the four-kaon invariant mass distribution for selected events. To determine the signal yield an unbinned maximum likelihood fit is performed. The $B_s^0 \rightarrow \phi\phi$ signal component is modelled by two Gaussian functions with a common mean. The resolution of the first Gaussian is measured from data to be $13.9 \pm 0.6 \text{ MeV}/c^2$. The relative fraction and resolution of the second Gaussian are fixed to 0.785 and $29.5 \text{ MeV}/c^2$ respectively, where values have been obtained from simulation. Combinatorial background is modelled using an exponential function. Background from $B^0 \rightarrow \phi K^{*0}$ and $B_s^0 \rightarrow K^{*0} \bar{K}^{*0}$ decays is found to be negligible both in simulation and data driven studies. Fitting the probability density function (PDF) described above to the data, a signal yield of 801 ± 29 events is found.

In addition to the dominant P-wave $\phi \rightarrow K^+K^-$ component described in Section 1, other contributions, either from $f_0 \rightarrow K^+K^-$ or non-resonant K^+K^- , are possible. The size of these contributions, neglecting interference effects, is studied by relaxing the ϕ

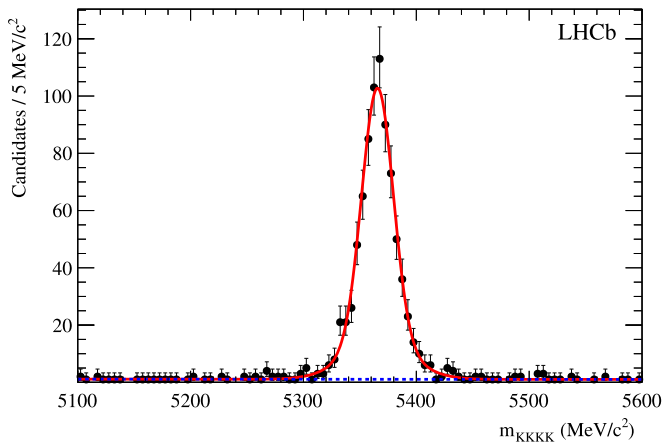


Fig. 2. Invariant $K^+K^-K^+K^-$ mass distribution for selected $B_s^0 \rightarrow \phi\phi$ candidates. A fit of a double Gaussian signal component together with an exponential background (dotted line) is superimposed.

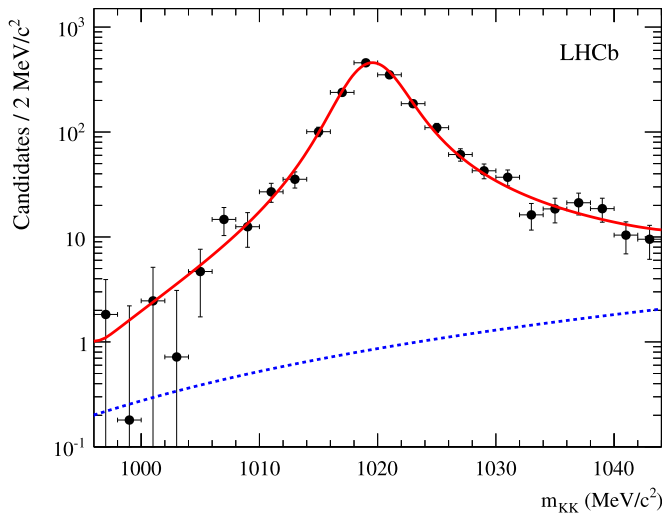


Fig. 3. Invariant mass distribution of K^+K^- pairs for the $B_s^0 \rightarrow \phi\phi$ data without a ϕ mass cut. The background has been removed using the s Plot technique in conjunction with the K^+K^- invariant mass. There are two entries per B_s^0 candidate. The solid line shows the result of the fit model described in the text. The fitted S-wave component is shown by the dotted line.

mass cut to be within $25 \text{ MeV}/c^2$ of the nominal value⁴ and using the s Plot technique in conjunction with the ϕ mass to subtract the combinatorial background.

The resulting ϕ mass distribution is shown in Fig. 3. A fit of a relativistic P-wave Breit–Wigner function together with a two body phase space component to model the S-wave contribution is superimposed. In a $\pm 25 \text{ MeV}/c^2$ mass window, the size of the S-wave component is found to be $(1.3 \pm 1.2)\%$. Since the S-wave yield is consistent with zero, it will be neglected in the following section. A systematic uncertainty arising from this assumption will be assigned.

4. Results

The polarization amplitudes ($|A_0|^2$, $|A_\perp|^2$, $|A_\parallel|^2$), are determined by performing an unbinned maximum likelihood fit to the reconstructed mass and helicity angle distributions. For each event,

Table 2

Measured polarization amplitudes and strong phase difference. The uncertainties are statistical only. The sum of the squared amplitudes is constrained to unity. The correlation coefficient between $|A_0|^2$ and $|A_\perp|^2$ is -0.47 .

Parameter	Measurement
$ A_0 ^2$	0.365 ± 0.022
$ A_\perp ^2$	0.291 ± 0.024
$ A_\parallel ^2 = 1 - (A_0 ^2 + A_\perp ^2)$	0.344 ± 0.024
$\cos(\delta_\parallel)$	-0.844 ± 0.068

the ϕ meson used to define θ_1 is chosen at random. Both the signal and background PDFs are the products of a mass component described in Section 3 together with an angular component. The angular component of the signal is given by Eq. (3) multiplied by the angular acceptance of the detector. The acceptance is determined using the simulation and is calculated separately according to trigger type, i.e. whether the event was triggered by the signal candidate or other particles in the event. In total the fit for the polarization amplitudes has eight free parameters: the signal angular parameters $|A_0|^2$, $|A_\perp|^2$ and $\cos(\delta_\parallel)$ defined in Section 1, the fractions of signal for each trigger type, the resolution of the core Gaussian, the B_s^0 mass and the slope of the mass background. The sum of squared amplitudes is constrained such that $|A_0|^2 + |A_\perp|^2 + |A_\parallel|^2 = 1$. The angular distributions for the background have been studied using the mass sidebands in the data, where mass sidebands are defined to be between 60 and 300 MeV/c^2 either side of the nominal B_s^0 mass [33]. With the current sample size these distributions are consistent with being flat in $(\cos\theta_1, \cos\theta_2, \Phi)$. Therefore, a uniform angular PDF is assumed and more complicated shapes are considered as part of the systematic studies. The values of $\Gamma_s = 0.657 \pm 0.009 \pm 0.008 \text{ ps}^{-1}$ and $\Delta\Gamma_s = 0.123 \pm 0.029 \pm 0.011 \text{ ps}^{-1}$ together with their correlation coefficient of -0.3 quoted in [23] are used as a Gaussian constraint. The validity of the fit model has been extensively tested using simulated data samples. The results are given in Table 2 and the angular projections are shown in Fig. 4.

Several sources of systematic uncertainty on the determination of the polarization amplitudes are considered and summarized in Table 3. With the present size of the dataset, the S-wave component is consistent with zero. From the studies described in Section 3 and fits to the data including the S-wave terms in the PDF [34], we consider a maximum S-wave component of 2%. Simulation studies have been performed to investigate the effect of neglecting an S-wave component of this size. As discussed in Section 1, the integration that leads to Eq. (5) assumes uniform time acceptance. This is not the case due to lifetime biasing cuts in the trigger and offline selections. The functional form of the decay time acceptance is obtained through the use of Monte Carlo events. The difference between using this functional form in simulation studies and using uniform time acceptance is taken as a systematic uncertainty. The uncertainty on the angular acceptance for the signal is propagated to the observables also using Monte Carlo studies. The analysis was repeated with an alternative background angular distribution, taken from a coarsely binned histogram in $(\cos\theta_1, \cos\theta_2, \Phi)$ of the mass sidebands, and the difference taken as a systematic uncertainty. An additional uncertainty arises from angular acceptance dependencies on trigger type. This dependency is corrected for using Monte Carlo events, with half of the effect on fitted parameters assigned as systematic uncertainties. The total systematic uncertainty is obtained from the sum in quadrature of the individual uncertainties.

The distributions of the U and V triple product observables are shown in Fig. 5 for the mass range $5286.6 < M(K^+K^-K^+K^-) < 5446.6 \text{ MeV}/c^2$. To determine the triple product asymmetries,

⁴ This is a larger window than the $\pm 12 \text{ MeV}/c^2$ window used in the polarization amplitude and strong phase difference measurements.

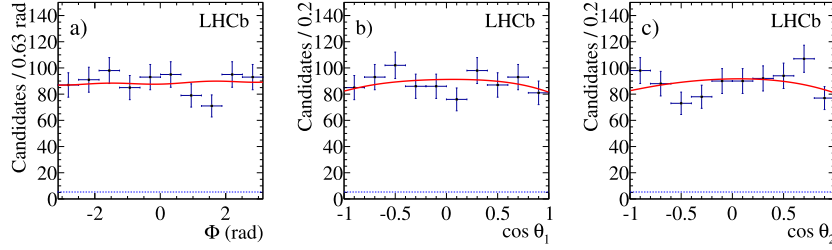


Fig. 4. Angular distributions for (a) Φ , (b) $\cos\theta_1$ and (c) $\cos\theta_2$ of $B_s^0 \rightarrow \phi\phi$ events with the fit projections for signal and background superimposed for the total fitted PDF (solid line) and background component (dotted line).

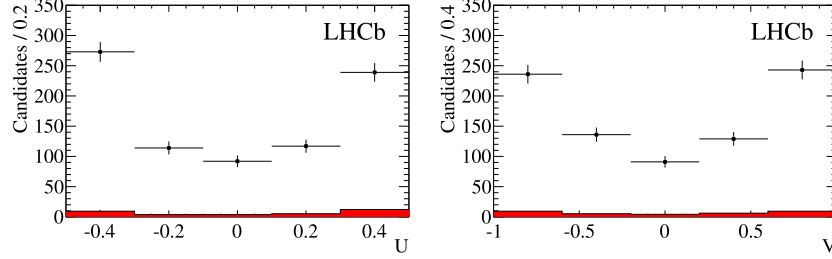


Fig. 5. Distributions of the U (left) and V (right) observables for the $B_s^0 \rightarrow \phi\phi$ data in the mass range $5286.6 < M(K^+K^-K^+K^-) < 5446.6$ MeV/ c^2 . The distribution for the background is taken from the mass sidebands, normalized to the same mass range and is shown by the solid histogram.

Table 3

Systematic uncertainties on the measured polarization amplitudes and the strong phase difference.

Source	$ A_0 ^2$	$ A_\perp ^2$	$ A_\parallel ^2$	$\cos\delta_\parallel$
S-wave component	0.007	0.005	0.012	0.001
Decay time acceptance	0.006	0.006	0.002	0.007
Angular acceptance	0.007	0.006	0.006	0.028
Trigger category	0.003	0.002	0.001	0.004
Background model	0.001	–	0.001	0.003
Total	0.012	0.010	0.014	0.029

the dataset is partitioned according to whether U (V) is less than or greater than zero. Simultaneous fits are performed to the mass distributions for each of the two partitions corresponding to each observable individually. In these fits, the mean and resolution of the Gaussian signal component together with the slope of the exponential background component are common parameters. The asymmetries are left as free parameters and are fitted for directly in the simultaneous fit. The measured values are

$$A_U = -0.055 \pm 0.036,$$

$$A_V = 0.010 \pm 0.036.$$

Systematic uncertainties due to the residual effect of the decay time, geometrical acceptance and the signal and background fit models have been evaluated and are summarized in Table 4. The effect of the decay time acceptance has been found using the same method as for the polarization amplitudes. The impact of angular acceptance on the measured values has been obtained from simplified simulation studies. The total systematic uncertainty is conservatively estimated by choosing the larger of the two individual systematic uncertainties on A_U and A_V . The contributions are combined in quadrature to determine the total systematic error. Various cross-checks of the stability of the result have been performed. For example, dividing the data according to how the event was triggered or by magnet polarity. No significant bias is observed in these studies.

Table 4

Systematic uncertainties on the triple product asymmetries A_U and A_V . The total uncertainty is the quadratic sum of the larger of the two components.

Source	A_U	A_V	Final uncertainty
Angular acceptance	0.009	0.006	0.009
Decay time acceptance	0.006	0.014	0.014
Fit model	0.004	0.005	0.005
Total		0.018	

5. Summary

The polarization amplitudes and strong phase difference in the $B_s^0 \rightarrow \phi\phi$ decay mode are measured to be

$$|A_0|^2 = 0.365 \pm 0.022 \text{ (stat)} \pm 0.012 \text{ (syst)},$$

$$|A_\perp|^2 = 0.291 \pm 0.024 \text{ (stat)} \pm 0.010 \text{ (syst)},$$

$$|A_\parallel|^2 = 0.344 \pm 0.024 \text{ (stat)} \pm 0.014 \text{ (syst)},$$

$$\cos(\delta_\parallel) = -0.844 \pm 0.068 \text{ (stat)} \pm 0.029 \text{ (syst)},$$

where the sum of the squared amplitudes is constrained to be unity. These values agree well with the CDF measurements [25]. Measurements in other $B \rightarrow VV$ penguin transitions at the B factories generally give higher values of f_L [9–14]. It is interesting to note that the value of f_L found in the $B_s^0 \rightarrow \phi\phi$ channel is almost equal to that in the $B_s^0 \rightarrow K^*0\bar{K}^{*0}$ decay [17]. The results are in agreement with QCD factorization predictions [6,7], but disfavour the pQCD estimate given in [8].

The triple product asymmetries in this mode are measured to be

$$A_U = -0.055 \pm 0.036 \text{ (stat)} \pm 0.018 \text{ (syst)},$$

$$A_V = 0.010 \pm 0.036 \text{ (stat)} \pm 0.018 \text{ (syst)}.$$

Both values are in good agreement with those reported by the CDF Collaboration [25] and consistent with the hypothesis of CP conservation.

Acknowledgements

We express our gratitude to our colleagues in the CERN accelerator departments for the excellent performance of the LHC. We thank the technical and administrative staff at CERN and at the LHCb institutes, and acknowledge support from the National Agencies: CAPES, CNPq, FAPERJ and FINEP (Brazil); CERN; NSFC (China); CNRS/IN2P3 (France); BMBF, DFG, HGF and MPG (Germany); SFI (Ireland); INFN (Italy); FOM and NWO (The Netherlands); SCSR (Poland); ANCS (Romania); MinES of Russia and Rosatom (Russia); MICINN, XuntaGal and GENCAT (Spain); SNSF and SER (Switzerland); NAS Ukraine (Ukraine); STFC (United Kingdom); NSF (USA). We also acknowledge the support received from the ERC under FP7 and the Region Auvergne.

Open access

This article is published Open Access at sciencedirect.com. It is distributed under the terms of the Creative Commons Attribution License 3.0, which permits unrestricted use, distribution, and reproduction in any medium, provided the original authors and source are credited.

References

- [1] M. Gronau, J.L. Rosner, Phys. Rev. D 84 (2011) 096013, arXiv:1107.1232.
- [2] W. Bensalem, D. London, Phys. Rev. D 64 (2001) 116003, arXiv:hep-ph/0005018.
- [3] A. Datta, D. London, Int. J. Mod. Phys. A 19 (2004) 2505, arXiv:hep-ph/0303159.
- [4] S. Nandi, A. Kundu, J. Phys. G 32 (2006) 835, arXiv:hep-ph/0510245.
- [5] A. Datta, M. Duraisamy, D. London, Phys. Lett. B 701 (2011) 357, arXiv:1103.2442.
- [6] M. Beneke, J. Rohrer, D. Yang, Nucl. Phys. B 774 (2007) 64, arXiv:hep-ph/0612290.
- [7] H.-Y. Cheng, C.-K. Chua, Phys. Rev. D 80 (2009) 114026, arXiv:0910.5237.
- [8] A. Ali, et al., Phys. Rev. D 76 (2007) 074018, arXiv:hep-ph/0703162.
- [9] Belle Collaboration, K.-F. Chen, et al., Phys. Rev. Lett. 94 (2005) 221804, arXiv:hep-ex/0503013.
- [10] BaBar Collaboration, B. Aubert, et al., Phys. Rev. Lett. 98 (2007) 051801, arXiv:hep-ex/0610073.
- [11] BaBar Collaboration, B. Aubert, et al., Phys. Rev. D 78 (2008) 092008, arXiv:0808.3586.
- [12] BaBar Collaboration, P. del Amo Sanchez, et al., Phys. Rev. D 83 (2011) 051101, arXiv:1012.4044.
- [13] Belle Collaboration, J. Zhang, et al., Phys. Rev. Lett. 95 (2005) 141801, arXiv:hep-ex/0408102.
- [14] BaBar Collaboration, B. Aubert, et al., Phys. Rev. Lett. 97 (2006) 201801, arXiv:hep-ex/0607057.
- [15] A.L. Kagan, Phys. Lett. B 601 (2004) 151, arXiv:hep-ph/0405134.
- [16] A. Datta, et al., Phys. Rev. D 76 (2007) 034015, arXiv:0705.3915.
- [17] LHCb Collaboration, R. Aaij, et al., Phys. Lett. B 709 (2012) 50, arXiv:1111.4183.
- [18] C.-W. Chiang, L. Wolfenstein, Phys. Rev. D 61 (2000) 074031, arXiv:hep-ph/9911338.
- [19] C.-W. Chiang, Phys. Rev. D 62 (2000) 014017, arXiv:hep-ph/0002243.
- [20] M. Raidal, Phys. Rev. Lett. 89 (2002) 231803, arXiv:hep-ph/0208091.
- [21] M. Bartsch, G. Buchalla, C. Kraus, $B \rightarrow V_L V_L$ decays at next-to-leading order in QCD, arXiv:0810.0249.
- [22] J. Charles, et al., Phys. Rev. D 84 (2011) 033005, arXiv:1106.4041.
- [23] LHCb Collaboration, R. Aaij, et al., Phys. Rev. Lett. 108 (2012) 101803, arXiv:1112.3183.
- [24] CDF Collaboration, D.E. Acosta, et al., Phys. Rev. Lett. 95 (2005) 031801, arXiv:hep-ex/0502044.
- [25] CDF Collaboration, T. Aaltonen, et al., Phys. Rev. Lett. 107 (2011) 261802, arXiv:1107.4999.
- [26] T. Sjöstrand, S. Mrenna, P. Skands, JHEP 0605 (2006) 026, arXiv:hep-ph/0603175.
- [27] I. Belyaev, et al., IEEE Nucl. Sci. Symp. Conf. Rec. (NSS/MIC) (2010) 1155.
- [28] D.J. Lange, Nucl. Instrum. Methods A 462 (2001) 152.
- [29] S. Agostinelli, et al., Nucl. Instrum. Methods A 506 (2003) 250.
- [30] LHCb Collaboration, A.A. Alves Jr., et al., JINST 3 (2008) S08005.
- [31] V. Gligorov, C. Thomas, M. Williams, LHCb Collaboration, The HLT inclusive B triggers, LHCb-PUB-2011-016.
- [32] M. Pivk, F.R. Le, Nucl. Instrum. Methods A 555 (2005) 356, arXiv:physics/0402083.
- [33] Particle Data Group, K. Nakamura, et al., J. Phys. G 37 (2010) 075021.
- [34] Y. Xie, P. Clarke, G. Cowan, F. Muheim, JHEP 0909 (2009) 074, arXiv:0908.3627.

LHCb Collaboration

R. Aaij³⁸, C. Abellan Beteta^{33,n}, B. Adeva³⁴, M. Adinolfi⁴³, C. Adrover⁶, A. Affolder⁴⁹, Z. Ajaltouni⁵, J. Albrecht³⁵, F. Alessio³⁵, M. Alexander⁴⁸, S. Ali³⁸, G. Alkhazov²⁷, P. Alvarez Cartelle³⁴, A.A. Alves Jr.²², S. Amato², Y. Amhis³⁶, J. Anderson³⁷, R.B. Appleby⁵¹, O. Aquines Gutierrez¹⁰, F. Archilli^{18,35}, A. Artamonov³², M. Artuso^{53,35}, E. Aslanides⁶, G. Auriemma^{22,m}, S. Bachmann¹¹, J.J. Back⁴⁵, V. Balagura^{28,35}, W. Baldini¹⁶, R.J. Barlow⁵¹, C. Barschel³⁵, S. Barsuk⁷, W. Barter⁴⁴, A. Bates⁴⁸, C. Bauer¹⁰, Th. Bauer³⁸, A. Bay³⁶, I. Bediaga¹, S. Belogurov²⁸, K. Belous³², I. Belyaev²⁸, E. Ben-Haim⁸, M. Benayoun⁸, G. Bencivenni¹⁸, S. Benson^{47,*}, J. Benton⁴³, R. Bernet³⁷, M.-O. Bettler¹⁷, M. van Beuzekom³⁸, A. Bien¹¹, S. Bifani¹², T. Bird⁵¹, A. Bizzeti^{17,h}, P.M. Bjørnstad⁵¹, T. Blake³⁵, F. Blanc³⁶, C. Blanks⁵⁰, J. Blouw¹¹, S. Blusk⁵³, A. Bobrov³¹, V. Bocci²², A. Bondar³¹, N. Bondar²⁷, W. Bonivento¹⁵, S. Borghi^{48,51}, A. Borgia⁵³, T.J.V. Bowcock⁴⁹, C. Bozzi¹⁶, T. Brambach⁹, J. van den Brand³⁹, J. Bressieux³⁶, D. Brett⁵¹, M. Britsch¹⁰, T. Britton⁵³, N.H. Brook⁴³, H. Brown⁴⁹, A. Büchler-Germann³⁷, I. Burducea²⁶, A. Bursche³⁷, J. Buytaert³⁵, S. Cadeddu¹⁵, O. Callot⁷, M. Calvi^{20,j}, M. Calvo Gomez^{33,n}, A. Camboni³³, P. Campana^{18,35}, A. Carbone¹⁴, G. Carboni^{21,k}, R. Cardinale^{19,35,i}, A. Cardini¹⁵, L. Carson⁵⁰, K. Carvalho Akiba², G. Casse⁴⁹, M. Cattaneo³⁵, Ch. Cauet⁹, M. Charles⁵², Ph. Charpentier³⁵, N. Chiapolini³⁷, K. Ciba³⁵, X. Cid Vidal³⁴, G. Ciezarek⁵⁰, P.E.L. Clarke⁴⁷, M. Clemencic³⁵, H.V. Cliff⁴⁴, J. Closier³⁵, C. Coca²⁶, V. Coco³⁸, J. Cogan⁶, P. Collins³⁵, A. Comerma-Montells³³, A. Contu⁵², A. Cook⁴³, M. Coombes⁴³, G. Corti³⁵, B. Couturier³⁵, G.A. Cowan³⁶, R. Currie⁴⁷, C. D'Ambrosio³⁵, P. David⁸, P.N.Y. David³⁸, I. De Bonis⁴, K. De Bruyn³⁸, S. De Capua^{21,k}, M. De Cian³⁷, J.M. De Miranda¹, L. De Paula², P. De Simone¹⁸, D. Decamp⁴, M. Deckenhoff⁹, H. Degaudenzi^{36,35}, L. Del Buono⁸, C. Deplano¹⁵, D. Derkach^{14,35}, O. Deschamps⁵, F. Dettori³⁹, J. Dickens⁴⁴, H. Dijkstra³⁵, P. Diniz Batista¹, F. Domingo Bonal^{33,n}, S. Donleavy⁴⁹, F. Dordei¹¹, A. Dosil Suárez³⁴, D. Dossett⁴⁵, A. Dovbnya⁴⁰, F. Dupertuis³⁶, R. Dzhelyadin³²,

A. Dziurda²³, S. Easo⁴⁶, U. Egede⁵⁰, V. Egorychev²⁸, S. Eidelman³¹, D. van Eijk³⁸, F. Eisele¹¹,
 S. Eisenhardt⁴⁷, R. Ekelhof⁹, L. Eklund⁴⁸, Ch. Elsasser³⁷, D. Elsby⁴², D. Esperante Pereira³⁴,
 A. Falabella^{16,14,e}, C. Färber¹¹, G. Fardell⁴⁷, C. Farinelli³⁸, S. Farry¹², V. Fave³⁶, V. Fernandez Albor³⁴,
 M. Ferro-Luzzi³⁵, S. Filippov³⁰, C. Fitzpatrick⁴⁷, M. Fontana¹⁰, F. Fontanelli^{19,i}, R. Forty³⁵, O. Francisco²,
 M. Frank³⁵, C. Frei³⁵, M. Frosini^{17,f}, S. Furcas²⁰, A. Gallas Torreira³⁴, D. Galli^{14,c}, M. Gandelman²,
 P. Gandini⁵², Y. Gao³, J.-C. Garnier³⁵, J. Garofoli⁵³, J. Garra Tico⁴⁴, L. Garrido³³, D. Gascon³³,
 C. Gaspar³⁵, R. Gauld⁵², N. Gauvin³⁶, M. Gersabeck³⁵, T. Gershon^{45,35}, Ph. Ghez⁴, V. Gibson⁴⁴,
 V.V. Gligorov³⁵, C. Göbel⁵⁴, D. Golubkov²⁸, A. Golutvin^{50,28,35}, A. Gomes², H. Gordon⁵²,
 M. Grabalosa Gándara³³, R. Graciani Diaz³³, L.A. Granado Cardoso³⁵, E. Graugés³³, G. Graziani¹⁷,
 A. Grecu²⁶, E. Greening⁵², S. Gregson⁴⁴, B. Gui⁵³, E. Gushchin³⁰, Yu. Guz³², T. Gys³⁵,
 C. Hadjivasiliou⁵³, G. Haefeli³⁶, C. Haen³⁵, S.C. Haines⁴⁴, T. Hampson⁴³, S. Hansmann-Menzemer¹¹,
 R. Harji⁵⁰, N. Harnew⁵², J. Harrison⁵¹, P.F. Harrison⁴⁵, T. Hartmann⁵⁵, J. He⁷, V. Heijne³⁸,
 K. Hennessy⁴⁹, P. Henrard⁵, J.A. Hernando Morata³⁴, E. van Herwijnen³⁵, E. Hicks⁴⁹, K. Holubyev¹¹,
 P. Hopchev⁴, W. Hulsbergen³⁸, P. Hunt⁵², T. Huse⁴⁹, R.S. Huston¹², D. Hutchcroft⁴⁹, D. Hynds⁴⁸,
 V. Iakovenko⁴¹, P. Ilten¹², J. Imong⁴³, R. Jacobsson³⁵, A. Jaeger¹¹, M. Jahjah Hussein⁵, E. Jans³⁸,
 F. Jansen³⁸, P. Jaton³⁶, B. Jean-Marie⁷, F. Jing³, M. John⁵², D. Johnson⁵², C.R. Jones⁴⁴, B. Jost³⁵,
 M. Kabbalo⁹, S. Kandybei⁴⁰, M. Karacson³⁵, T.M. Karbach⁹, J. Keaveney¹², I.R. Kenyon⁴², U. Kerzel³⁵,
 T. Ketel³⁹, A. Keune³⁶, B. Khanji⁶, Y.M. Kim⁴⁷, M. Knecht³⁶, R.F. Koopman³⁹, P. Koppenburg³⁸,
 M. Korolev²⁹, A. Kozlinskiy³⁸, L. Kravchuk³⁰, K. Kreplin¹¹, M. Kreps⁴⁵, G. Krocker¹¹, P. Krokovny³¹,
 F. Kruse⁹, K. Kruzelecki³⁵, M. Kucharczyk^{20,23,35,j}, V. Kudryavtsev³¹, T. Kvaratskheliya^{28,35},
 V.N. La Thi³⁶, D. Lacarrere³⁵, G. Lafferty⁵¹, A. Lai¹⁵, D. Lambert⁴⁷, R.W. Lambert³⁹, E. Lanciotti³⁵,
 G. Lanfranchi¹⁸, C. Langenbruch³⁵, T. Latham⁴⁵, C. Lazzeroni⁴², R. Le Gac⁶, J. van Leerdam³⁸,
 J.-P. Lees⁴, R. Lefèvre⁵, A. Leflat^{29,35}, J. Lefrançois⁷, O. Leroy⁶, T. Lesiak²³, L. Li³, L. Li Gioi⁵, M. Lieng⁹,
 M. Liles⁴⁹, R. Lindner³⁵, C. Linn¹¹, B. Liu³, G. Liu³⁵, J. von Loeben²⁰, J.H. Lopes², E. Lopez Asamar³³,
 N. Lopez-March³⁶, H. Lu³, J. Luisier³⁶, A. Mac Raighne⁴⁸, F. Machefert⁷, I.V. Machikhiliyan^{4,28},
 F. Maciuc¹⁰, O. Maev^{27,35}, J. Magnin¹, S. Malde⁵², R.M.D. Mamunur³⁵, G. Manca^{15,d}, G. Mancinelli⁶,
 N. Mangiafave⁴⁴, U. Marconi¹⁴, R. Märki³⁶, J. Marks¹¹, G. Martellotti²², A. Martens⁸, L. Martin⁵²,
 A. Martín Sánchez⁷, M. Martinelli³⁸, D. Martinez Santos³⁵, A. Massafferri¹, Z. Mathe¹², C. Matteuzzi²⁰,
 M. Matveev²⁷, E. Maurice⁶, B. Maynard⁵³, A. Mazurov^{16,30,35}, G. McGregor⁵¹, R. McNulty¹²,
 M. Meissner¹¹, M. Merk³⁸, J. Merkel⁹, S. Miglioranzi³⁵, D.A. Milanese¹³, M.-N. Minard⁴,
 J. Molina Rodriguez⁵⁴, S. Monteil⁵, D. Moran¹², P. Morawski²³, R. Mountain⁵³, I. Mous³⁸, F. Muheim⁴⁷,
 K. Müller³⁷, R. Muresan²⁶, B. Muryn²⁴, B. Muster³⁶, J. Mylroie-Smith⁴⁹, P. Naik⁴³, T. Nakada³⁶,
 R. Nandakumar⁴⁶, I. Nasteva¹, M. Needham⁴⁷, N. Neufeld³⁵, A.D. Nguyen³⁶, C. Nguyen-Mau^{36,o},
 M. Nicol⁷, V. Niess⁵, N. Nikitin²⁹, T. Nikodem¹¹, A. Nomerotski^{52,35}, A. Novoselov³²,
 A. Oblakowska-Mucha²⁴, V. Obraztsov³², S. Oggero³⁸, S. Ogilvy⁴⁸, O. Okhrimenko⁴¹, R. Oldeman^{15,35,d},
 M. Orlandea²⁶, J.M. Otalora Goicochea², P. Owen⁵⁰, B.K. Pal⁵³, J. Palacios³⁷, A. Palano^{13,b}, M. Palutan¹⁸,
 J. Panman³⁵, A. Papanestis⁴⁶, M. Pappagallo⁴⁸, C. Parkes⁵¹, C.J. Parkinson⁵⁰, G. Passaleva¹⁷,
 G.D. Patel⁴⁹, M. Patel⁵⁰, S.K. Paterson⁵⁰, G.N. Patrick⁴⁶, C. Patrignani^{19,i}, C. Pavel-Nicorescu²⁶,
 A. Pazos Alvarez³⁴, A. Pellegrino³⁸, G. Penso^{22,l}, M. Pepe Altarelli³⁵, S. Perazzini^{14,c}, D.L. Perego^{20,j},
 E. Perez Trigo³⁴, A. Pérez-Calero Yzquierdo³³, P. Perret⁵, M. Perrin-Terrin⁶, G. Pessina²⁰, A. Petrolini^{19,i},
 A. Phan⁵³, E. Picatoste Olloqui³³, B. Pie Valls³³, B. Pietrzyk⁴, T. Pilař⁴⁵, D. Pinci²², R. Plackett⁴⁸,
 S. Playfer⁴⁷, M. Plo Casasus³⁴, G. Polok²³, A. Poluektov^{45,31}, E. Polycarpo², D. Popov¹⁰, B. Popovici²⁶,
 C. Potterat³³, A. Powell⁵², J. Prisciandaro³⁶, V. Pugatch⁴¹, A. Puig Navarro³³, W. Qian⁵³,
 J.H. Rademacker⁴³, B. Rakotomiaramanana³⁶, M.S. Rangel², I. Raniuk⁴⁰, G. Raven³⁹, S. Redford⁵²,
 M.M. Reid⁴⁵, A.C. dos Reis¹, S. Ricciardi⁴⁶, A. Richards⁵⁰, K. Rinnert⁴⁹, D.A. Roa Romero⁵, P. Robbe⁷,
 E. Rodrigues^{48,51}, F. Rodrigues², P. Rodriguez Perez³⁴, G.J. Rogers⁴⁴, S. Roiser³⁵, V. Romanovsky³²,
 M. Rosello^{33,n}, J. Rouvinet³⁶, T. Ruf³⁵, H. Ruiz³³, G. Sabatino^{21,k}, J.J. Saborido Silva³⁴, N. Sagidova²⁷,
 P. Sail⁴⁸, B. Saitta^{15,d}, C. Salzmann³⁷, M. Sannino^{19,i}, R. Santacesaria²², C. Santamarina Rios³⁴,
 R. Santinelli³⁵, E. Santovetti^{21,k}, M. Sapunov⁶, A. Sarti^{18,l}, C. Satriano^{22,m}, A. Satta²¹, M. Savrie^{16,e},
 D. Savrina²⁸, P. Schaack⁵⁰, M. Schiller³⁹, H. Schindler³⁵, S. Schleich⁹, M. Schlupp⁹, M. Schmelling¹⁰,
 B. Schmidt³⁵, O. Schneider³⁶, A. Schopper³⁵, M.-H. Schune⁷, R. Schwemmer³⁵, B. Sciascia¹⁸,
 A. Sciubba^{18,l}, M. Seco³⁴, A. Semennikov²⁸, K. Senderowska²⁴, I. Sepp⁵⁰, N. Serra³⁷, J. Serrano⁶,

P. Seyfert¹¹, M. Shapkin³², I. Shapoval^{40,35}, P. Shatalov²⁸, Y. Shcheglov²⁷, T. Shears⁴⁹, L. Shekhtman³¹, O. Shevchenko⁴⁰, V. Shevchenko²⁸, A. Shires⁵⁰, R. Silva Coutinho⁴⁵, T. Skwarnicki⁵³, N.A. Smith⁴⁹, E. Smith^{52,46}, K. Sobczak⁵, F.J.P. Soler⁴⁸, A. Solomin⁴³, F. Soomro^{18,35}, B. Souza De Paula², B. Spaan⁹, A. Sparkes⁴⁷, P. Spradlin⁴⁸, F. Stagni³⁵, S. Stahl¹¹, O. Steinkamp³⁷, S. Stoica²⁶, S. Stone^{53,35}, B. Storaci³⁸, M. Straticiuc²⁶, U. Straumann³⁷, V.K. Subbiah³⁵, S. Swientek⁹, M. Szczekowski²⁵, P. Szczypka³⁶, T. Szumlak²⁴, S. T'Jampens⁴, E. Teodorescu²⁶, F. Teubert³⁵, C. Thomas⁵², E. Thomas³⁵, J. van Tilburg¹¹, V. Tisserand⁴, M. Tobin³⁷, S. Tolk³⁹, S. Topp-Joergensen⁵², N. Torr⁵², E. Tournefier^{4,50}, S. Tourneur³⁶, M.T. Tran³⁶, A. Tsaregorodtsev⁶, N. Tuning³⁸, M. Ubeda Garcia³⁵, A. Ukleja²⁵, U. Uwer¹¹, V. Vagnoni¹⁴, G. Valenti¹⁴, R. Vazquez Gomez³³, P. Vazquez Regueiro³⁴, S. Vecchi¹⁶, J.J. Velthuis⁴³, M. Veltri^{17,g}, B. Viaud⁷, I. Videau⁷, D. Vieira², X. Vilasis-Cardona^{33,n}, J. Visniakov³⁴, A. Vollhardt³⁷, D. Volyanskyy¹⁰, D. Voong⁴³, A. Vorobyev²⁷, V. Vorobyev³¹, H. Voss¹⁰, R. Waldi⁵⁵, S. Wandernoth¹¹, J. Wang⁵³, D.R. Ward⁴⁴, N.K. Watson⁴², A.D. Webber⁵¹, D. Websdale⁵⁰, M. Whitehead⁴⁵, D. Wiedner¹¹, L. Wiggers³⁸, G. Wilkinson⁵², M.P. Williams^{45,46}, M. Williams⁵⁰, F.F. Wilson⁴⁶, J. Wishahi⁹, M. Witek²³, W. Witzeling³⁵, S.A. Wotton⁴⁴, K. Wyllie³⁵, Y. Xie⁴⁷, F. Xing⁵², Z. Xing⁵³, Z. Yang³, R. Young⁴⁷, O. Yushchenko³², M. Zangoli¹⁴, M. Zavertyaev^{10,a}, F. Zhang³, L. Zhang⁵³, W.C. Zhang¹², Y. Zhang³, A. Zhelezov¹¹, L. Zhong³, A. Zvyagin³⁵

¹ Centro Brasileiro de Pesquisas Físicas (CBPF), Rio de Janeiro, Brazil

² Universidade Federal do Rio de Janeiro (UFRJ), Rio de Janeiro, Brazil

³ Center for High Energy Physics, Tsinghua University, Beijing, China

⁴ LAPP, Université de Savoie, CNRS/IN2P3, Annecy-Le-Vieux, France

⁵ Clermont Université, Université Blaise Pascal, CNRS/IN2P3, LPC, Clermont-Ferrand, France

⁶ CPPM, Aix-Marseille Université, CNRS/IN2P3, Marseille, France

⁷ LAL, Université Paris-Sud, CNRS/IN2P3, Orsay, France

⁸ LPNHE, Université Pierre et Marie Curie, Université Paris Diderot, CNRS/IN2P3, Paris, France

⁹ Fakultät Physik, Technische Universität Dortmund, Dortmund, Germany

¹⁰ Max-Planck-Institut für Kernphysik (MPIK), Heidelberg, Germany

¹¹ Physikalisches Institut, Ruprecht-Karls-Universität Heidelberg, Heidelberg, Germany

¹² School of Physics, University College Dublin, Dublin, Ireland

¹³ Sezione INFN di Bari, Bari, Italy

¹⁴ Sezione INFN di Bologna, Bologna, Italy

¹⁵ Sezione INFN di Cagliari, Cagliari, Italy

¹⁶ Sezione INFN di Ferrara, Ferrara, Italy

¹⁷ Sezione INFN di Firenze, Firenze, Italy

¹⁸ Laboratori Nazionali dell'INFN di Frascati, Frascati, Italy

¹⁹ Sezione INFN di Genova, Genova, Italy

²⁰ Sezione INFN di Milano Bicocca, Milano, Italy

²¹ Sezione INFN di Roma Tor Vergata, Roma, Italy

²² Sezione INFN di Roma La Sapienza, Roma, Italy

²³ Henryk Niewodniczanski Institute of Nuclear Physics Polish Academy of Sciences, Kraków, Poland

²⁴ AGH University of Science and Technology, Kraków, Poland

²⁵ Soltan Institute for Nuclear Studies, Warsaw, Poland

²⁶ Horia Hulubei National Institute of Physics and Nuclear Engineering, Bucharest-Magurele, Romania

²⁷ Petersburg Nuclear Physics Institute (PNPI), Gatchina, Russia

²⁸ Institute of Theoretical and Experimental Physics (ITEP), Moscow, Russia

²⁹ Institute of Nuclear Physics, Moscow State University (SINP MSU), Moscow, Russia

³⁰ Institute for Nuclear Research of the Russian Academy of Sciences (INR RAN), Moscow, Russia

³¹ Budker Institute of Nuclear Physics (SB RAS) and Novosibirsk State University, Novosibirsk, Russia

³² Institute for High Energy Physics (IHEP), Protvino, Russia

³³ Universitat de Barcelona, Barcelona, Spain

³⁴ Universidad de Santiago de Compostela, Santiago de Compostela, Spain

³⁵ European Organization for Nuclear Research (CERN), Geneva, Switzerland

³⁶ Ecole Polytechnique Fédérale de Lausanne (EPFL), Lausanne, Switzerland

³⁷ Physik-Institut, Universität Zürich, Zürich, Switzerland

³⁸ Nikhef National Institute for Subatomic Physics, Amsterdam, The Netherlands

³⁹ Nikhef National Institute for Subatomic Physics and VU University Amsterdam, Amsterdam, The Netherlands

⁴⁰ NSC Kharkiv Institute of Physics and Technology (NSC KIPT), Kharkiv, Ukraine

⁴¹ Institute for Nuclear Research of the National Academy of Sciences (KINR), Kyiv, Ukraine

⁴² University of Birmingham, Birmingham, United Kingdom

⁴³ H.H. Wills Physics Laboratory, University of Bristol, Bristol, United Kingdom

⁴⁴ Cavendish Laboratory, University of Cambridge, Cambridge, United Kingdom

⁴⁵ Department of Physics, University of Warwick, Coventry, United Kingdom

⁴⁶ STFC Rutherford Appleton Laboratory, Didcot, United Kingdom

⁴⁷ School of Physics and Astronomy, University of Edinburgh, Edinburgh, United Kingdom

⁴⁸ School of Physics and Astronomy, University of Glasgow, Glasgow, United Kingdom

⁴⁹ Oliver Lodge Laboratory, University of Liverpool, Liverpool, United Kingdom

⁵⁰ Imperial College London, London, United Kingdom

⁵¹ School of Physics and Astronomy, University of Manchester, Manchester, United Kingdom

⁵² Department of Physics, University of Oxford, Oxford, United Kingdom

⁵³ Syracuse University, Syracuse, NY, United States

⁵⁴ Pontifícia Universidade Católica do Rio de Janeiro (PUC-Rio), Rio de Janeiro, Brazil^p

⁵⁵ Institut für Physik, Universität Rostock, Rostock, Germany^q

* Corresponding author.

E-mail address: sean.benson@cern.ch (S. Benson).

^a P.N. Lebedev Physical Institute, Russian Academy of Science (LPI RAS), Moscow, Russia.

^b Università di Bari, Bari, Italy.

^c Università di Bologna, Bologna, Italy.

^d Università di Cagliari, Cagliari, Italy.

^e Università di Ferrara, Ferrara, Italy.

^f Università di Firenze, Firenze, Italy.

^g Università di Urbino, Urbino, Italy.

^h Università di Modena e Reggio Emilia, Modena, Italy.

ⁱ Università di Genova, Genova, Italy.

^j Università di Milano Bicocca, Milano, Italy.

^k Università di Roma Tor Vergata, Roma, Italy.

^l Università di Roma La Sapienza, Roma, Italy.

^m Università della Basilicata, Potenza, Italy.

ⁿ LIFAELS, La Salle, Universitat Ramon Llull, Barcelona, Spain.

^o Hanoi University of Science, Hanoi, Viet Nam.

^p Associated to: Universidade Federal do Rio de Janeiro (UFRJ), Rio de Janeiro, Brazil.

^q Associated to: Physikalisches Institut, Ruprecht-Karls-Universität Heidelberg, Heidelberg, Germany.